



Sharif University of Technology  
**Scientia Iranica**  
*Transactions F: Nanotechnology*  
<http://scientiairanica.sharif.edu>



# MHD Carreau nanofluid with Arrhenius activation energy in a porous medium

S. Hussain, S.M. Atif\*, M. Sagheer, and M.A. Manzoor

*Department of Mathematics, Capital University of Science and Technology, Islamabad, Pakistan.*

Received 15 September 2021; received in revised form 14 June 2022; accepted 29 August 2022

## KEYWORDS

MHD Carreau nanofluid;  
 Convective heat transfer;  
 Arrhenius activation energy;  
 Porous sheet.

**Abstract.** In this investigation, the combined effects of magnetohydrodynamic and Arrhenius activation energy on Carreau nanofluid past a nonlinear stretching sheet are examined. Buongiorno nanofluid model is considered to study the impact of nanoparticles with a porous medium. To analyze the modeled problem, this study incorporates convective heating mode and heat source/sink. With the help of appropriate similarity transformations, formulated Partial Differential Equations (PDEs) are transmuted into nonlinear Ordinary Differential Equations (ODEs). The solution of the resulting ODEs is achieved via shooting technique. In the limiting case, the results are numerically computed and compared with the already reported results for the validity of the MATLAB code, and splendid agreement is found between the results. Variations in fluid motion, temperature, and concentration due to changes in different parameters are analyzed graphically and discussed in detail. Our simulations reveal that the temperature profile increases following an increase in the Biot number, Arrhenius energy parameter, and magnetic number. According to the results, the skin friction coefficient is enhanced at higher values of the stretching parameter. Moreover, the enhancement of skin friction coefficient is more in shear thickening behavior as compared to shear thinning behavior of the fluid.

© 2022 Sharif University of Technology. All rights reserved.

## 1. Introduction

In engineering and industrial processes, it is of significance to analyze fluid flow. Metal, extrusion, spinning, wired drawing, manufacturing of rubber sheets, food manufacturing, and cooling of vast metallic plates like electrolyte are common examples. In recent time, numerous researchers [1–4] have taken measures to investigate the phenomenon of fluid flow through the stretching surface. They studied that the implementation of magnetic field would result in the slowness of

the fluid motion. The small solid particle is termed as nanoparticle; such nanoparticles range from 1 to 100 nanometers in size. In 1995, Choi and Eastman [5] put forward the term nanofluid in their pioneering work. Due to the corresponding prospective engineering application, various researchers performed many detailed studies on this topic. Nanotechnology has a vast range of applications in the fields of science and technology in modern developments. Recently, the improvement in nanotechnology has increased exponentially. Malvandi and Ganji [6] observed the studied forced convection phenomenon in a channel containing nanoparticles. They analyzed that the suction from the surface enhanced the Nusselt number, while the blowing was reduced. The critical observation done on the characteristics of nanofluids was conducted

\*. *Corresponding author.*  
*E-mail address: siratif@hotmail.com (S.M. Atif)*

by Khanafer and Vafai [7]. They found that the viscosity of effective nanofluids increased as the volume fraction was enhanced, whereas it decreased with an increment in the temperature. Furthermore, Cu-H<sub>2</sub>O on a porous surface was discussed by Sureshkumar and Muthamilselvan [8]. The analysis of the driven cavity flow with various properties of heat exchange in nanofluid was carried out in [9,10]. Recently, the nanofluid flow through various shape geometries has caught noticeable attention from different fields. The effect of spatial fractional heat conduction in the magnetohydrodynamic (MHD) boundary layer flow using Gr-Fe<sub>3</sub>O<sub>4</sub>-H<sub>2</sub>O hybrid nanofluid was investigated by Khazayinejad and Nourazar [11]. Megahed [12] studied the Carreau fluid flow due to a nonlinearly stretching sheet with thermal radiation, heat flux, and variable conductivity. Atif et al. [13–15] observed the tangent hyperbolic nanofluid flow past a linear stretching surface, wedge, and paraboloid surface. Hsiao [16] carried out electrical magnetohydrodynamics Carreau and micropolar nanofluid flow with the impact of different parameters. Micropolar nanofluid with modified Fourier and Fick's law was ascertained by Atif et al. [17]. Using porous media, further experiments were performed to study the boundary layer flow past a nonlinear stretched sheet [18–21].

The analysis of peristaltic motion in Carreau fluid with chemical reactions has motivated the researchers to analyze its usage in industry, engineering, and medical science like biochemistry, diagnostic therapy, neurology, and treatment for cancer. The Carreau model [22] falls into the category of non-Newtonian fluid models with high and low shear rates for which the constituent relationship accumulates. To explain non-Newtonian fluids, several experimental terms have been proposed based on various characteristics obtained by Bird [23]. Due to the distinct application of Carreau model in engineering and technology, various researchers have worked on properties of such model types. Atif et al. [24] illustrated the behavior of Carreau fluid flow past a channel in the presence of microcantilever sensor. Moreover, different researchers have investigated the Carreau fluid model for dealing with various flow problems [25,26]. Martins et al. [27] investigated the numerical analysis of shear thinning axisymmetric flow impacts of a Carreau fluid. Olajuwon [28] numerically illustrated the heat and mass exchange in a hydromagnetic Carreau fluid with radiation and thermal diffusion. Atif et al. [29] studied the micropolar Carreau nanofluid with thermal radiation effects. Tshela [30] analyzed the free surface of the Carreau fluid flowing down on an inclined plane. Mathematical analysis of Carreau fluid flow and heat transfer within an eccentric catheterized artery was conducted by Alsemiry et al. [31]. Numerical analysis of Carreau fluid flow over a vertical porous

microchannel with entropy generation was carried out by Reedy et al. [32]. One of the main observations was that the entropy generation was reduced with an increase in the Weissenberg number.

Recently, the convective flow of Ag-water MHD nanofluid was studied by Thangavelu et al. [33]. Selimli et al. [34] performed the MHD numerical analyses of hydrodynamically developing laminar liquid lithium duct flow. MHD dissipative Casson fluid with variable properties was analyzed by Idowu et al. [35]. One of the key observations was that the variable viscosity reduced the fluid motion near the surface where it is accelerated away from the surface. Combined effects of magnetic and electrical fields on the hydrodynamic and thermophysical parameters of magneto-viscous fluid flow were ascertained by Selimli et al. [36]. The effect of the carbon nanotubes (CNT) on MHD nanofluid past a stretchable rotating disk was analyzed by Iqbal et al. [37] and it was concluded that an increase in the CNT in base fluid would enhance the heat transfer rate. Darcy-Forchheimer MHD Jeffery nanofluid flow past a permeable cone was presented by Gupta et al. [38]. One of the main observations was that the fluid motion hiked with an increase in the value of the porosity parameter. Gopal et al. [39] ascertained the EMHD nanofluid flow under the effect of higher-order chemical reaction. Thermo-bioconvective transport of magneto-Casson nanofluid over a wedge containing motile microorganisms and variable thermal conductivity was analyzed by Waqas et al. [40]. Rout and Mishra [41] studied the energy transport phenomenon in MHD nanofluid flow over a stretching surface. One of the key observations was that the surface heat flux increased following an increase in the value of the radiation parameter.

Based on a review of the literature, it came to our attention that MHD Carreau nanofluid flow past a nonlinear porous stretching sheet with Arrhenius activation energy has not been studied yet. For the efficient heat transfer phenomenon, Joule heating and heat generation/absorption have been incorporated into the energy equation. The governing Partial Differential Equations (PDEs) of momentum, temperature, and concentration are transformed into Ordinary Differential Equations (ODEs) by means of similarity transformations. The system of nonlinear ODEs is solved using shooting method together with RK4. Matlab code is verified by reproducing already published results. The graphs are used to study the variations due to governing parameters including temperature, velocity, and concentration distribution.

## 2. Mathematical model

A two-dimensional MHD Carreau nanofluid past a nonlinear stretching sheet in a porous medium was

considered. The sheet was stretched with velocity  $u_w(x) = bx^m$  in a region  $y > 0$ , where  $b$  and  $m$  are the positive constant and stretching parameter, respectively. The surface temperature is considered as  $T_w$  and fluid's temperature is taken as  $T_f$ . No nanoparticles in the flux condition are considered at the boundary, meaning that the fluid is strongly affected by thermophoresis. Fluid is subjected to temperature gradient; at an extremely large value of  $y$ , the nanoparticles concentration and temperature are assumed constant and are denoted by  $C_\infty$  and  $T_\infty$ , respectively. Along  $y$ -axis, a magnetic field having  $B_0$  strength is implemented, as illustrated in Figure 1.

In the light of the above assumptions the equations describing the motion, temperature and concentration are as follows:

$$u_x + v_y = 0, \tag{1}$$

$$uu_x + vv_y = \nu u_{yy} \left[ 1 + \Gamma^2(u_y)^2 \right]^{\frac{n-1}{2}} + \nu(n-1)\Gamma^2 u_{yy}(u_y)^2 \left[ 1 + \Gamma^2(u_y)^2 \right]^{\frac{n-3}{2}} - \left( \frac{\nu}{k} \right) u - \frac{\sigma B_0^2 u}{\rho}, \tag{2}$$

$$uT_x + vT_y = \alpha T_{yy} + \tau \left[ D_B C_y T_y + \frac{D_T}{T_\infty} (T_y)^2 \right] + \frac{Q_0}{(\rho c_p)_f} (T - T_\infty) + \frac{\sigma B_0^2 u^2}{\rho c_p}, \tag{3}$$

$$uC_x + vC_y = D_B C_{yy} + \frac{D_T}{T_\infty} T_{yy} - R_1(C - C_\infty) \left( \frac{T}{T_\infty} \right)^m \exp\left(-\frac{E^*}{K^*T}\right). \tag{4}$$

The boundary conditions are:

$$u = u_w(x) = bx^m, \quad v = 0, \quad kT_y = -h_f(T_w - T),$$

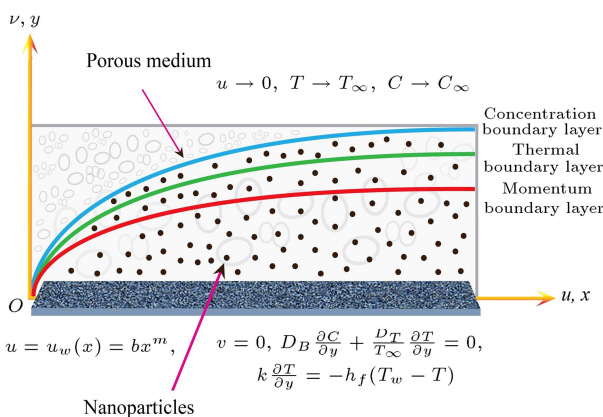


Figure 1. Flow configuration.

$$D_B C_y + \frac{D_T}{T_\infty} T_y = 0 \quad \text{at} \quad y = 0, \\ u \rightarrow 0, \quad T \rightarrow T_\infty, \\ C \rightarrow C_\infty \quad \text{as} \quad y \rightarrow \infty. \tag{5}$$

We convert PDEs and these boundary conditions into the ODEs by adopting the following similarity variable [42].

$$\psi(x, y) = \sqrt{\frac{2\nu b}{m+1}} x^{\frac{m+1}{2}} f(\eta), \\ \eta = y \sqrt{\frac{b(m+1)}{2\nu}} x^{\frac{m-1}{2}}, \\ \theta(\eta) = \frac{T - T_\infty}{T_w - T_\infty}, \quad \phi(\eta) = \frac{C - C_\infty}{C_w - C_\infty}. \tag{6}$$

The continuity equation is automatically satisfied and Eqs. (2)–(4) yield the following:

$$\left[ 1 + nW_e^2 f'^2 \right] \left[ 1 + W_e^2 f'^2 \right]^{\frac{n-3}{2}} f''' + f'' f - \frac{2}{m+1} \left[ m f'^2 + K_1 f' \right] - M f' = 0, \tag{7}$$

$$\frac{\theta''}{Pr} + N_t \theta^2 + N_b \phi' \theta' + \frac{2\theta\lambda}{(m+1)} + M E c f'^2 + f \theta' = 0, \tag{8}$$

$$\phi'' + \frac{N_t}{N_b} \theta'' + Le Pr f \phi' - \frac{2}{m+1} \gamma_1 \phi Le Pr (1 + \gamma_2 \theta(\eta))^m e^{\left(\frac{-E}{1+\gamma_2\theta}\right)} = 0. \tag{9}$$

The associated BCs are:

$$f(\eta) = 0, \quad f'(\eta) = 1, \quad \theta'(\eta) = Bi(\theta(\eta) - 1), \\ N_b \phi'(\eta) + N_t \theta'(\eta) = 0, \quad \text{at} \quad \eta = 0, \\ f' \rightarrow 0, \quad \theta \rightarrow 0, \quad \phi \rightarrow 0 \quad \text{as} \quad \eta \rightarrow \infty, \tag{10}$$

where:

- $K_1 = \frac{\nu}{k(bu_w^{m-1})^{\frac{1}{m}}}$ : The porosity parameter;
- $\lambda = \frac{Q_0}{(\rho c_p)_f (bu_w^{m-1})^{\frac{1}{m}}}$ : Heat source if  $\lambda > 0$  and sink parameter if  $\lambda < 0$ ;
- $Pr = \frac{\nu}{\alpha}$ : The Prandtl number;
- $E = \frac{E^*}{T_\infty K^*}$ : The Arrhenius activation energy parameter;
- $Nt = \frac{(\rho c_p)_p D_T (T_w - T_\infty)}{(\rho c_p)_f \nu_f T_\infty}$ : Thermophoresis parameter;

- $W_e^2 = \frac{b^3(m+1)\Gamma^2}{2\nu} x^{3m-1}$ : The Weissenberg number;
- $Le = \frac{\alpha}{D_B}$ : Lewis number;
- $\gamma_1 = \frac{\nu R_1}{D_B(bu_w^{m-1})^{\frac{1}{m}}}$ : Chemical reaction parameter;
- $M = \frac{2\sigma B_0^2}{\rho(m+1)bx^{m-1}}$ : The magnetic parameter;
- $Bi = \frac{h_f}{x^{\frac{m-1}{2}} K \sqrt{\frac{b(m+1)}{2\nu}}}$ : The Biot number;
- $Nb = \frac{(\rho c_p)_p D_B(C_w - C_\infty)}{(\rho c_p)_f \nu_f}$ : The Brownian motion parameter;
- $Ec = \frac{b^2 x^{2m}}{c_p(T_w - T_\infty)}$ : The Eckert number.

The skin friction coefficient  $Cf_x$ , heat transfer coefficient  $Nu_x$  and mass transfer coefficient  $Sh_x$  in the dimensional form are as follows:

$$Cf_x = \frac{\tau_w}{\rho u_w^2}, \quad Nu_x = \frac{xq_w}{k(T_w - T_\infty)},$$

$$Sh_x = \frac{xq_m}{D_B(C_w - C_\infty)}. \tag{11}$$

In the non-dimensional form, we have:

$$Cf_x Re_e^{\frac{1}{2}} = \sqrt{\frac{m+1}{2}} f''(0) \left[ 1 + W_e^2 (f''(0))^2 \right]^{\frac{n-1}{2}},$$

$$Nu_x Re_e^{-\frac{1}{2}} = -\sqrt{\frac{m+1}{2}} \theta'(0),$$

$$Sh_x Re_e^{-\frac{1}{2}} = -\sqrt{\frac{m+1}{2}} \phi'(0). \tag{12}$$

### 3. Implementation of the method

The modeled equations along with the BCs are tackled via the shooting technique. For this purpose, the new variables are introduced  $\varrho_1 = f$ ,  $\varrho_2 = f'$ ,  $\varrho_3 = f''$ ,  $\varrho_4 = \theta$ ,  $\varrho_5 = \theta'$ ,  $\varrho_6 = \phi$ , and  $\varrho_7 = \phi'$ .

$$\varrho'_1 = \varrho_2, \quad \varrho'_2 = \varrho_3,$$

$$\varrho'_3 = \frac{1}{[1 + nW_e^2 \varrho_3^2] [1 + W_e^2 \varrho_3^2]^{\frac{n-3}{2}}}$$

$$\left[ \frac{2}{m+1} (m\varrho_2^2 + K_1 \varrho_2) + M y_2 - \varrho_1 \varrho_3 \right]$$

$$\varrho'_4 = \varrho_5,$$

$$\varrho'_5 = -Pr \left[ \varrho_1 \varrho_5 + \frac{2\lambda}{m+1} \varrho_4 + Nb \varrho_7 \varrho_5 \right. \\ \left. + Nt \varrho_5^2 + MEc \varrho_5^2 \right]$$

$$\varrho'_6 = \varrho_7,$$

$$\varrho'_7 = -PrLe \varrho_1 \varrho_7 - \frac{Nt}{Nb} \varrho'_5 + \frac{2}{m+1} PrLe \gamma_1 \varrho_6$$

$$(1 + \gamma_2 \varrho_4)^m \exp\left(-\frac{E}{1 + \gamma_2 \varrho_4}\right), \tag{13}$$

with boundary conditions:

$$\varrho_1 = 0, \quad \varrho_2 = 1, \quad \varrho_5 = Bi(\varrho_4 - 1),$$

$$\varrho_7 = -\frac{Nt}{Nb} \varrho_5 \quad \text{at } \eta = 0,$$

$$\varrho_2 \rightarrow 0, \quad \varrho_4 \rightarrow 0,$$

$$\varrho_6 \rightarrow 0, \quad \text{as } \eta \rightarrow \infty. \tag{14}$$

To solve the above system of seven first-order ordinary differential Eq. (13), with the assistance of the shooting method, seven initial conditions are required. Therefore, we guess the three unknown conditions as  $\varrho_3(0) = s_1$ ,  $\varrho_4(0) = s_2$ , and  $\varrho_6(0) = s_3$ . The suitable guesses for  $s_1$ ,  $s_2$ , and  $s_3$  are chosen, such that the three known boundary conditions are approximately satisfied for  $\eta \rightarrow \infty$ . The Newton’s iterative scheme is applied to improve the accuracy of the initial guesses  $s_1$ ,  $s_2$ , and  $s_3$  until the desired approximation is met. In the computations for the rest of this article,  $\chi$  has been chosen as  $10^{-6}$ . The computations at different values of the emerging physical parameters have been performed over the appropriate bounded domain  $\eta_{max}$  instead of  $[0, \infty)$ . It is observed that at the increasing high values of  $\eta_{max}$ , there is no significant change observed in the results. The stopping criterion for the iterative process is:

$$\max\{|\varrho_2(\eta_{max}) - 0|, |\varrho_4(\eta_{max}) - 0|, |\varrho_6(\eta_{max}) - 0|\} < \chi,$$

where  $\chi$  is a very small positive real number.

#### 3.1. Code validation

To check the correctness of the code, the numerical values of the Nusselt number are reproduced, as reported by Hashim and Khan [25] in the literature and presented in Table 1. These assessments indicate the admirable agreement.

### 4. Results and discussions

Table 2 is organized to analyze the effect of governing parameters like  $m, M, W_e, K_1$  on skin friction coefficient ( $Cf_x Re_x^{1/2}$ ). Both shear thinning  $n < 1$  and shear thickening  $n > 1$  behaviors were analyzed. From this table, it was observed that the skin friction coefficient was enhanced at higher values of  $m, M$ , and  $W_e$ . It was also observed that the enhancement of the skin friction was greater due to the shear thickening behavior than the shear thinning behavior. The value of the skin friction coefficient decreased upon increase in the values of  $K_1$ .

Numerical simulations were performed for different physical parameters in governing equations of the

**Table 1.** Comparative values for  $-\theta'(0)$  at different values of  $Pr, N_t, Le$  when  $W_e = 3, N_b = 0.5, \lambda = \gamma = K_1 = 0$ .

$Pr$	$N_t$	$Le$	$m$	$-\theta'(0)$			
				Hashim & Khan [25]		Present study	
				$n = 0.5$	$n = 1.5$	$n = 0.5$	$n = 1.5$
1	0.1	1	2	0.6140	0.7354	0.6140	0.7354
			3	1.2440	1.4198	1.2440	1.4198
			5	1.6635	1.8615	1.2440	1.4198
	0.3			0.9215	1.0758	0.9215	1.0758
		0.5		0.8727	1.0243	0.8727	1.0243
		0.7		0.8252	0.9738	0.8252	0.9738
	0.1	0.5		0.9808	1.1379	0.9808	1.1379
		1.5		0.9649	1.1209	0.9649	1.1209
		2.5		0.9563	1.1114	0.9563	1.1114
		1	1	0.8144	0.9314	0.8144	0.9314
			2	1.10776	1.1295	1.10776	1.1295
			0.5	1.3406	1.5785	1.3406	1.5785

**Table 2.** Numerical outcomes of skin friction coefficient  $Cf_x Re_x^{\frac{1}{2}}$ .

$M$	$W_e$	$m$	$K_1$	$-Cf_x Re_x^{\frac{1}{2}}$	
				$n = 0.5$	$n = 1.5$
1	0.5	2	1	1.48601	1.55860
			1.5	1.69785	1.80263
			2	1.88115	2.02062
	1			1.39580	1.62546
		2		1.21203	1.75787
		3		1.08336	1.86797
	0.5	1		0.98379	1.01772
		2		1.48601	1.55860
		3		1.85515	1.95890
		2	1	1.48601	1.55860
			2	1.13297	1.16820
			3	0.64842	0.65751

MHD Carreau nanofluid with activation energy. For the whole study, the considered standard parameters are  $Pr = m = 2, Bi = Le = 1, W_e = 3, \gamma_1 = N_t = \lambda = 0.1, N_b = 0.5, E = 0.2, Ec = K_1 = 0.5,$  and  $\gamma_2 = 0.9,$  unless mentioned otherwise. All the simulations were performed for both shear thickening and thinning effects of Carreau nanofluid.

Figures 2–4 illustrate the impact of porosity parameter  $K_1$  on velocity  $f'(\eta),$  temperature  $\theta(\eta),$  and concentration  $\phi(\eta)$  profiles for dilatant and pseudoplas-

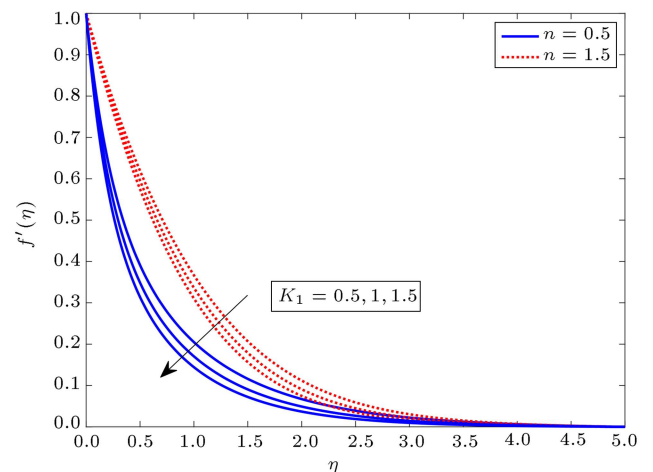


**Figure 2.** Variation in  $f'(\eta)$  caused by  $K_1$ .

tic nanofluids. It was found that with an increase in the value of porosity parameter  $K_1, f'(\eta)$  was reduced. However,  $\theta(\eta)$  and  $\phi(\eta)$  profiles increased following the rise in the values of porosity parameter  $K_1.$  Figures 5 and 6 show the effect of magnetic parameter  $M$  on  $f'(\eta), \theta(\eta),$  and  $\phi(\eta).$  It is noticeable that velocity  $f'(\eta)$  is continuously reduced by boosting  $M.$  Increasing the value of  $M$  usually creates Lorentz force by which  $\theta(\eta)$  is increased, as shown in Figure 6. Physically, larger values of  $M$  are indicative of a higher opposing force due to which the thickness of nanofluid boundary layer and  $\theta(\eta)$  is upsurged. Figure 7 shows the impact of  $\gamma_1$  on  $\phi(\eta).$  From these curves, it can be seen that the larger values of  $\gamma_1$  result in a decline in the chemical molecular diffusion; hence,  $\phi(\eta)$  is reduced.

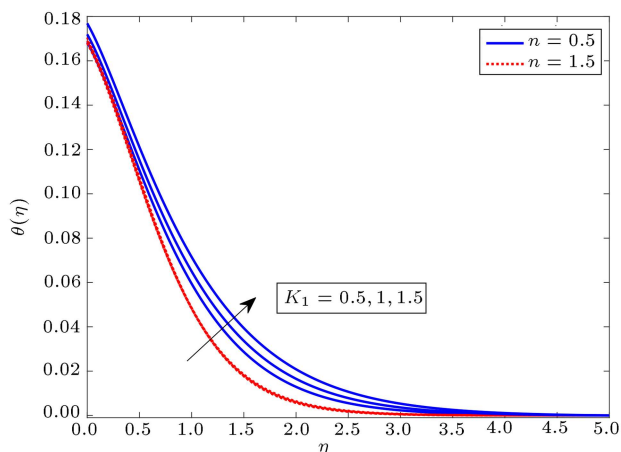


Figure 3. Variation in  $K_1$  caused by  $\theta(\eta)$ .

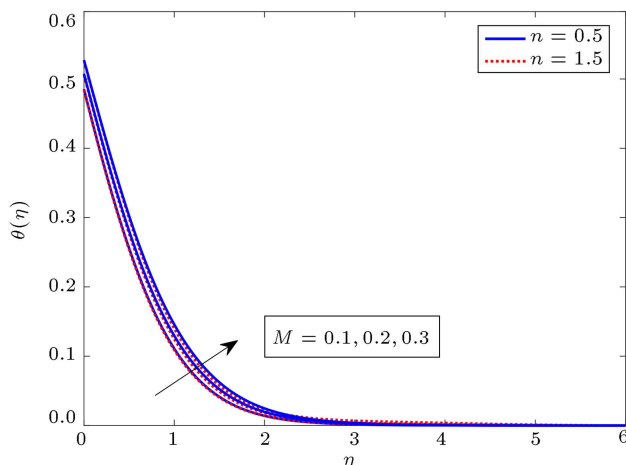


Figure 6. Variation in  $\theta(\eta)$  caused by  $M$ .

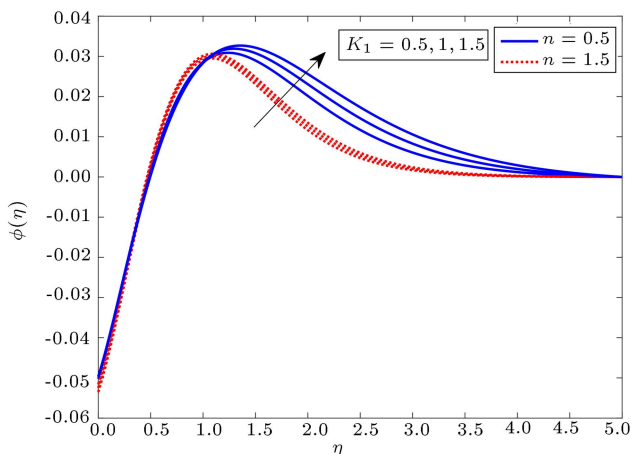


Figure 4. Variation in  $\phi(\eta)$  caused by  $K_1$ .

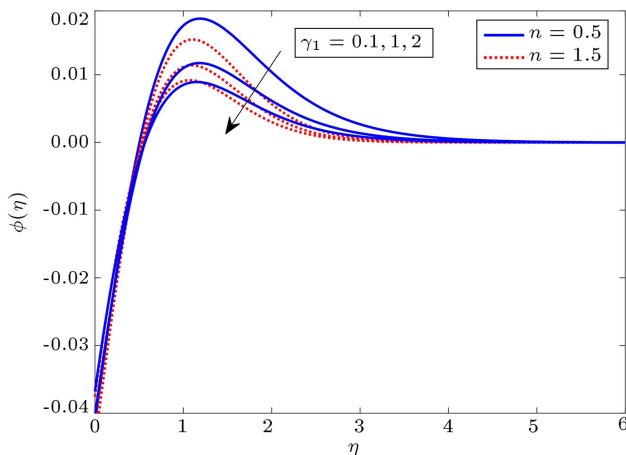


Figure 7. Variation in  $\phi(\eta)$  caused by  $\gamma_1$ .

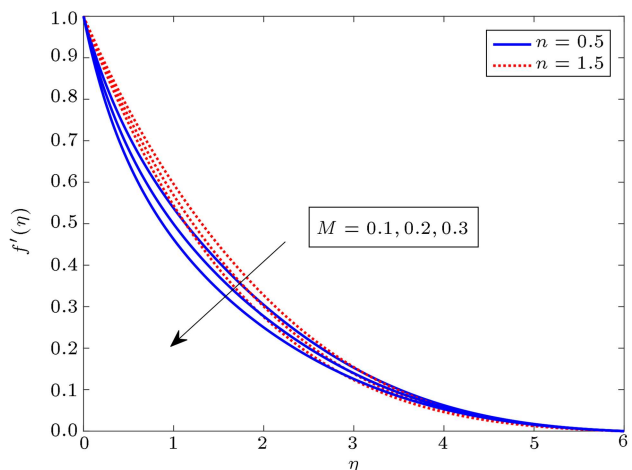


Figure 5. Variation in  $f'(\eta)$  caused by  $M$ .

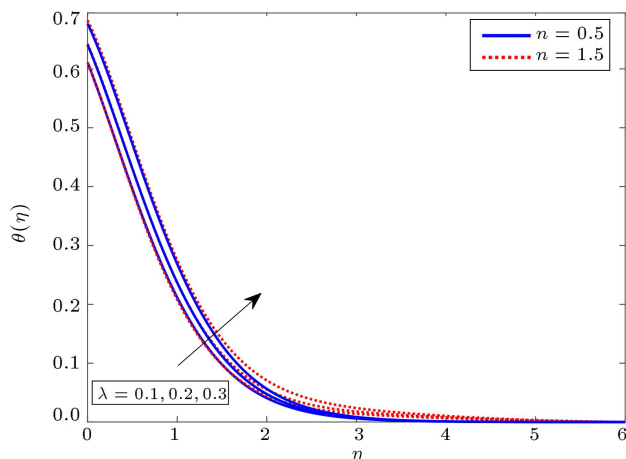


Figure 8. Variation in  $\theta(\eta)$  caused by  $\lambda > 0$ .

Figures 8–11 study the effect of heat source  $\lambda > 0$  and heat sink parameter  $\lambda < 0$  on temperature distribution  $\theta(\eta)$  and concentration distribution  $\phi(\eta)$  for dilatant and pseudoplastic nanofluids. Increasing values of  $\lambda > 0$  increases both temperature and concentration distribution, as presented in Figures 8

and 9. However, the inverse trend is seen for heat sinking parameter  $\lambda < 0$ , as shown in Figures 10 and 11. Figures 12 and 13 show a relationship among the Biot number  $Bi$ , energy  $\theta(\eta)$ , and concentration  $\phi(\eta)$ . Both  $\theta(\eta)$  and  $\phi(\eta)$  experience a rise following an increase in the value of  $Bi$ . Increase in the  $Bi$

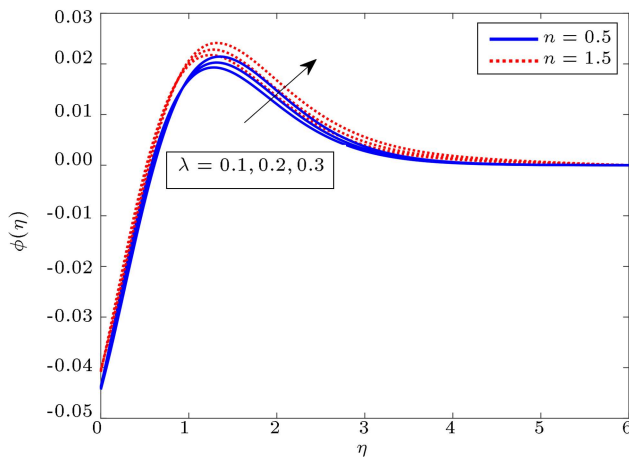


Figure 9. Variation in  $\phi(\eta)$  in  $\lambda > 0$ .

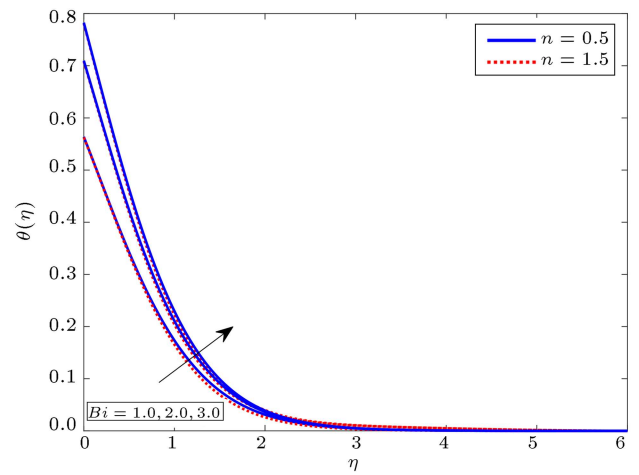


Figure 12. Variation in  $\theta(\eta)$  caused by  $Bi$ .

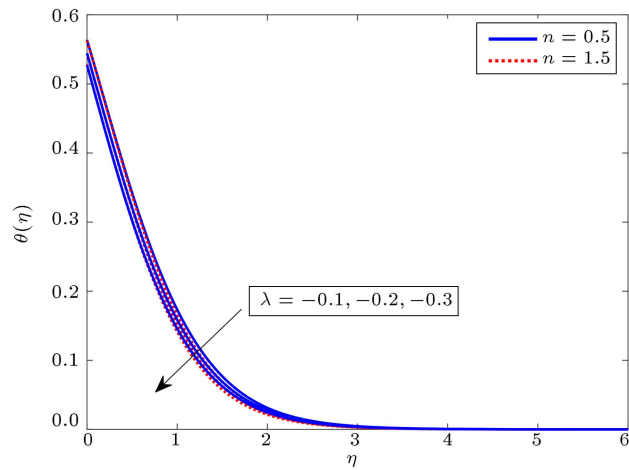


Figure 10. Variation in  $\theta(\eta)$  caused by  $\lambda < 0$ .

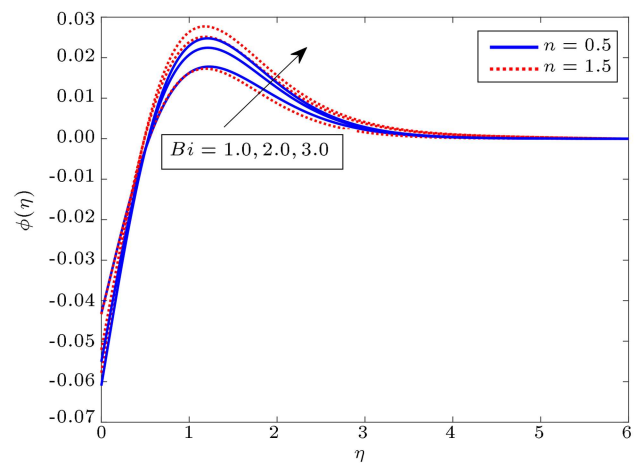


Figure 13. Variation in  $\phi(\eta)$  caused by  $Bi$ .

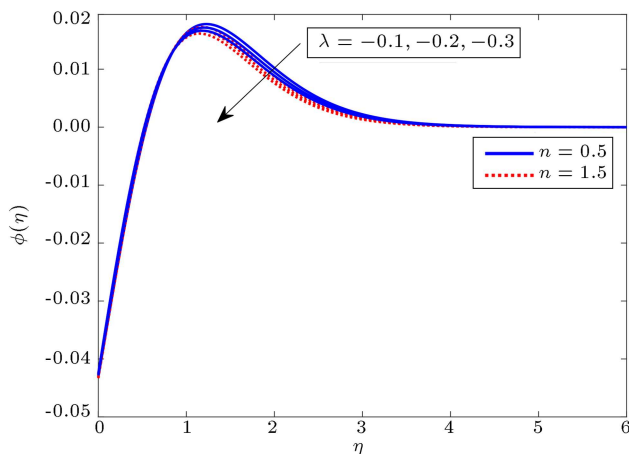


Figure 11. Variation in  $\phi(\eta)$  caused by  $\lambda < 0$ .

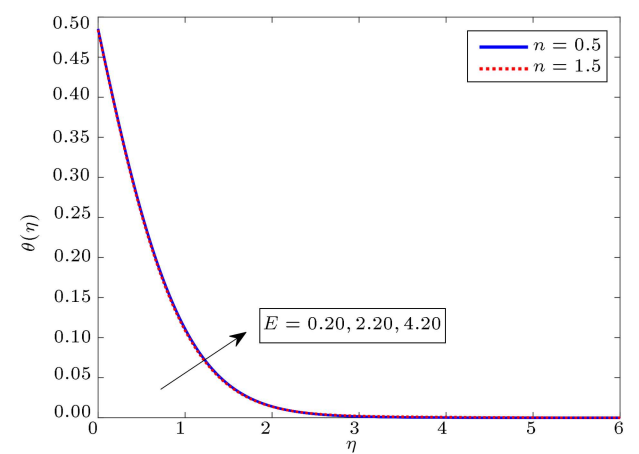


Figure 14. Variation in  $\theta(\eta)$  caused by  $E$ .

value causes a decline in the conductivity of the fluid, leading to the rise of  $\theta(\eta)$  and the concentration profile  $\phi(\eta)$ . The effect of Arrhenius activation energy  $E$  on temperature distribution  $\theta(\eta)$  and the concentration profile  $\phi(\eta)$  is shown in Figures 14 and 15. Figure 14 shows that  $\theta(\eta)$  increases with a rise in the value of  $E$ .

The concentration profile rises following the increase of  $E$  value. Accordingly, the above findings point to the increased concentration of the modified Arrhenius structure. Therefore, the overall chemical reaction is escalated, as presented in Figure 15. The  $Ec$  results for  $f'(\eta)$  and  $\theta(\eta)$  are characterized in Figures 16 and

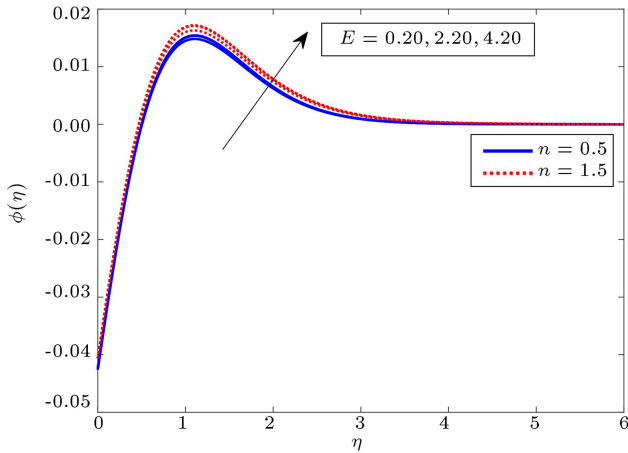


Figure 15. Variation in  $\phi(\eta)$  caused by  $E$ .

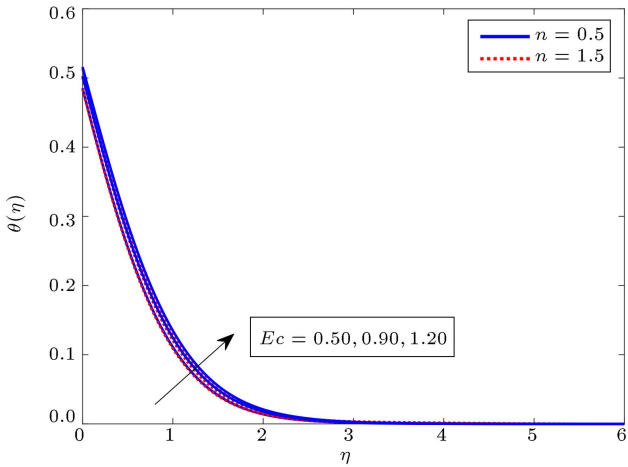


Figure 16. Variation in  $\theta(\eta)$  caused by  $Ec$ .

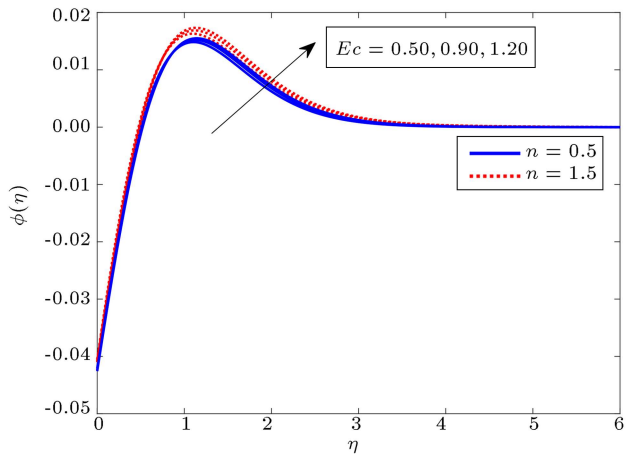


Figure 17. Variation in  $\phi(\eta)$  caused by  $Ec$ .

17. The kinetic energy of the fluid particle increases as  $Ec$  assumes a high value. It is observed that an increment in  $Ec$  results in a hike in  $\theta(\eta)$ . Therefore, the velocity and temperature of the fluids climb slightly and the thickness of the related boundary layer increases. Physically, dissipation increases upon raising

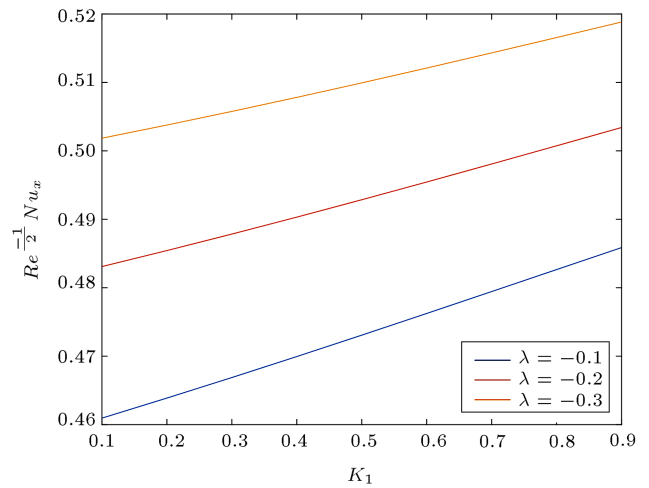


Figure 18. Variation in  $Nu_x Re_x^{-1/2}$  caused by  $\lambda < 0$  and  $K_1$  with  $n = 0.5$ .

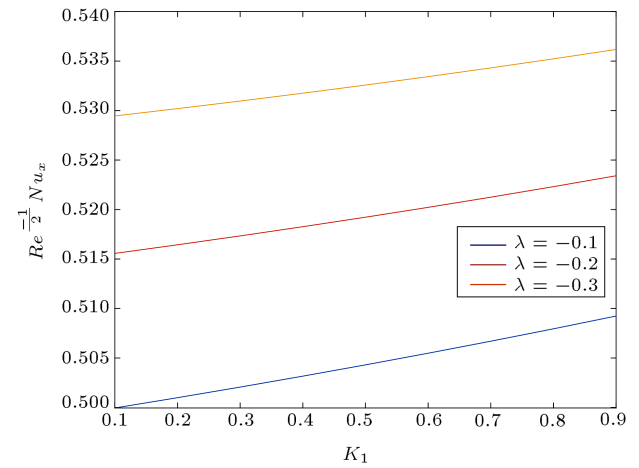
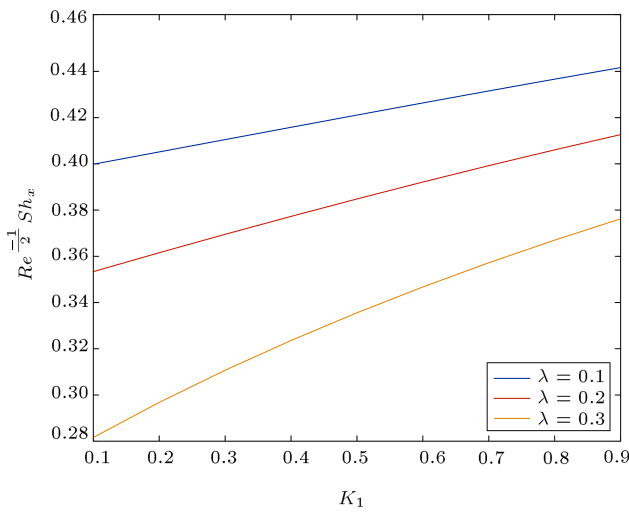


Figure 19. Variation in  $Nu_x Re_x^{-1/2}$  caused by  $\lambda < 0$  and  $K_1$  with  $n = 1.5$ .

$Ec$  values due to increase in the dissipation of internal fluid energy. Figure 17 is sketched for analysis of  $Ec$  effect on the concentration profile. The concentration profile is clearly increasing due to increase in  $Ec$ . The increase in the value of  $Ec$  is due to the rise of the fluid thermal energy. However, in case of shear thinning behavior, the thickness of the concentration boundary layer is higher than the shear thickening nanofluid.

Figures 18 and 19 represents the variation in Nusselt number due to porosity parameter and distinct values of chemical reaction parameter for both cases  $n = 0.5$  and  $n = 1.5$ . It is concluded that as the values of  $K_1$  and  $\lambda$  increase, the magnitude of  $Nu_x Re_x^{-1/2}$  is enhanced. Figures 20 and 21 display the variation in Sherwood number with respect to  $K_1$  at different values of  $\lambda > 0$ . It is noticeable that increase in each of  $K_1$  and  $\lambda > 0$  induces a decrement in  $Sh_x Re_x^{-1/2}$ . Figures 22 and 23 represent the fluctuation in the mass transfer rate with  $K_1$  at higher values of  $\lambda$  as well as with the values of  $n = 0.5$  and  $n = 1.5$ . It is clear that



**Figure 20.** Variation in  $Sh_x Re_x^{-1/2}$  caused by  $\lambda > 0$  and  $K_1$  with  $n = 0.5$ .

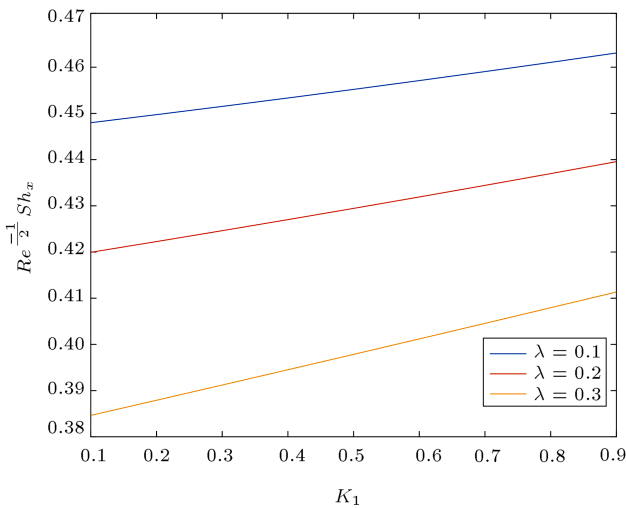


**Figure 21.** Variation in  $Sh_x Re_x^{-1/2}$  caused by  $\lambda > 0$  and  $K_1$  with  $n = 1.5$ .

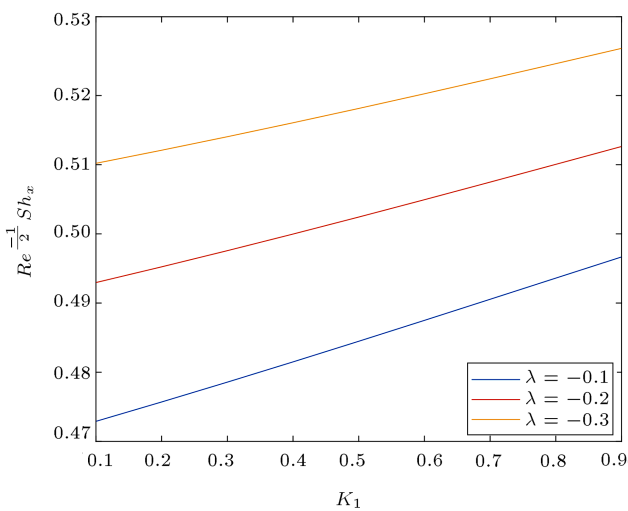


**Figure 22.** Variation in  $Sh_x Re_x^{-1/2}$  caused by  $\lambda < 0$  and  $K_1$  with  $n = 0.5$ .

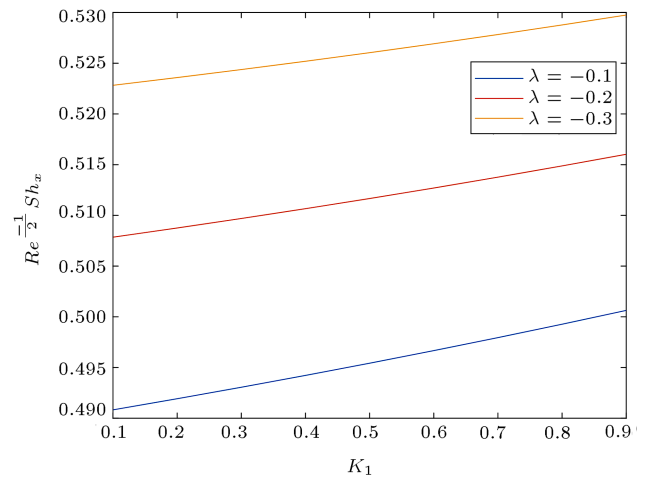


**Figure 23.** Variation in  $Sh_x Re_x^{-1/2}$  caused by  $\lambda < 0$  and  $K_1$  with  $n = 1.5$ .

increase in  $\lambda$  causes  $Sh_x Re_x^{-1/2}$  to decrease, whereas it increases as the porosity parameter is enhanced.

### 5. Conclusion

In this study, a computational investigation of magnetohydrodynamic (MHD) Carreau nanofluid flow in a porous medium was carried out with heat source/sink and chemical reaction. The main observations of this numerical study are as follows:

- $f'$  was enhanced as  $K_1$  increased, whereas it decreased as  $M$  rose;
- A decrement in the concentration was observed because of rising values of  $\lambda > 0$ ,  $K_1$ , and  $\lambda < 0$ ;
- The concentration  $\phi(\eta)$  fell at a larger estimation of chemical reaction;
- The skin friction coefficient was enhanced upon increasing the values of  $m$ ,  $M$ , and  $W_e$ . It was also observed that the enhancement of the skin friction was greater in the case of shear thickening behavior than the shear thinning behavior.

### Nomenclature

$b$	Constant
$Bi$	Biot number
$C$	Nanoparticle volume fraction
$C_p$	Specific heat
$C_w$	Concentration at the surface
$C_\infty$	Ambient Volume Concentration
$Cf_x$	Skin friction coefficient
$D_B$	Brownian diffusion
$D_T$	Thermophoresis
$f$	Dimensionless stream function

$h_f$	Heat transfer coefficient
$K$	Permeability of porous medium
$K_1$	Porosity parameter
$k$	Thermal conductivity
Le	Lewis number
$m$	Stretching parameter
$n$	Power law index
$N_b$	Brownian motion parameter
$N_t$	Thermophoresis parameter
Pr	Prandtl number
$Q_0$	Heat absorption/generation coefficient
$R_1$	Chemical reaction
$Re_a$	Local Reynolds number
$T$	Temperature of fluid
$T_\infty$	Ambient temperature
$T_w$	Temperature on the surface
$u, v$	Velocity components
$u_w$	Stretching sheet velocity
$W_e$	Weissenberg number
$x, y$	Space coordinates
$M$	Magnetic field parameter
$Sh_x$	Local Sherwood number
$Nu_x$	Local Nusselt Number
$Ec$	Eckert Number
$E$	Activation Energy

### Greek symbols

$\alpha$	Thermal diffusivity
$\lambda$	Heat source
$\gamma_1$	Chemical reaction parameter
$\theta$	Nondimensional temperature
$\sigma$	Electrical conductivity
$\mu$	Dynamic viscosity
$\sigma^*$	Stefan-Boltzmann constant
$\Delta T$	Temperature gradient
$\gamma_2$	Temperature difference parameter
$\rho$	Density
$\nu$	Kinematic viscosity
$\Gamma$	Relaxation parameter
$(\rho c_f)$	Heat capacity of the base fluid
$(\rho c_p)$	Heat capacity of the nanoparticle
$\mu$	Viscosity
$\mu_0$	Zero shear viscosity
$\mu_\infty$	Infinity shear viscosity
$\psi$	Stream function
$\eta$	Dimensionless similarity variable

$\theta$	Dimensionless temperature
$\phi$	Dimensionless concentration
$\tau$	The ratio of heat capacities
$\tau_w$	Surface shear stress

### References

1. Shehzad, S., Abdullah, Z., Abbasi, F., et al. "Magnetic field effect in three-dimensional flow of an Oldroyd-B nanofluid over a radiative surface", *Magnetism and Magnetic Materials*, **399**, pp. 97–108 (2016).
2. Zheng, L., Niu, J., Zhang, X., et al. "MHD flow and heat transfer over a porous shrinking surface with velocity slip and temperature jump", *Mathematical and Computer Modelling*, **56**(5–6), pp. 133–144 (2012).
3. Gireesha, B., Chamkha, A., Manjunatha, S., et al. "Mixed convective flow of a dusty fluid over a vertical stretching sheet with non uniform heat source/sink and radiation", *International Journal of Numerical Methods for Heat & Fluid Flow*, **45**(2), pp. 757–786 (2013).
4. Atif, S.M., Abbas, M., Rashid, U., et al. "Stagnation point flow of EMHD micropolar nanofluid with mixed convection and slip boundary", *Complexity*, **2021** (2021).
5. Choi, S.U. and Eastman, J.A. "Enhancing thermal conductivity of fluids with nanoparticles", Technical Report, Argonne National Lab., IL (United States) (1995).
6. Malvandi, A. and Ganji, D. "Effects of nanoparticle migration on force convection of alumina/water nanofluid in a cooled parallel-plate channel", *Advanced Powder Technology*, **25**(4), pp. 1369–1375 (2014).
7. Khanafer, K. and Vafai, K. "A critical synthesis of thermophysical characteristics of nanofluids", *International Journal of Heat and Mass Transfer*, **54**(19–20), pp. 4410–4428 (2011).
8. Sureshkumar, S. and Muthtamilselvan, M. "A slanted porous enclosure filled with Cu-water nanofluid", *The European Physical Journal Plus*, **131**(4), p. 95 (2016).
9. Chen, X., Li, J.M., Dai, W.T., et al. "Enhancing convection heat transfer in mini tubes with nanoparticle suspensions", *Journal of Engineering Thermophysics*, **25**(4), pp. 643–645 (2004).
10. Vishnuvardhanarao, E. and Das, M.K. "Laminar mixed convection in a parallel two sided lid-driven differentially heated square cavity filled with a fluid-saturated porous medium", *Numerical Heat Transfer Part A: Applications*, **53**(1), pp. 88–110 (2007).
11. Khazayinejad, M. and Nourazar, S. "On the effect of spatial fractional heat conduction in MHD boundary layer flow using  $Gr-Fe_3O_4-H_2O$  hybrid nanofluid", *International Journal of Thermal Sciences*, **172**, 107265 (2022).
12. Megahed, A.M. "Carreau fluid flow due to nonlinearly stretching sheet with thermal radiation, heat flux,

- and variable conductivity”, *Applied Mathematics and Mechanics*, **40**, pp. 1615–1624 (2019).
13. Atif, S.M., Hussain, S., and Sagheer, M. “Heat and mass transfer analysis of time dependent tangent hyperbolic nanofluid flow past a wedge”, *Physics Letters A*, **383**(11), pp. 1187–1198 (2019).
  14. Atif, S.M., Hussain, S., and Sagheer, M. “Effect of viscous dissipation and Joule heating on MHD radiative tangent hyperbolic nanofluid with convective and slip conditions”, *Journal of the Brazilian Society of Mechanical Sciences and Engineering*, **41**(4), pp. 189–206 (2019).
  15. Atif, S.M., Khan, W.A., Abbas, M., et al. “Bioconvection magnetohydrodynamic tangent hyperbolic nanofluid flow with quartic chemical reaction past a paraboloid surface”, *Computer Modeling in Engineering & Sciences*, **130**(1), pp. 205–220 (2022).
  16. Hsiao, K.L. “Stagnation electrical MHD nanofluid mixed convection with slip boundary on a stretching sheet”, *Applied Thermal Engineering*, **98**, pp. 850–861 (2016).
  17. Atif, S.M., Kamran, A., and Shah, S. “MHD micropolar nanofluid with non Fourier and non Fick’s law”, *International Communications in Heat and Mass Transfer*, **122**, p. 105114 (2021).
  18. Hady, F., Eid, M.R., and Ahmed, M.A. “A nanofluid flow in a nonlinear stretching surface saturated in a porous medium with yield stress effect”, *Applied Mathematics and Information Science Letters*, **2**(2), pp. 43–51 (2014).
  19. Seth, G.S., Bhattacharyya, A., Kumar, R., et al. “Modelling and numerical simulation of hydromagnetic natural convection Casson fluid flow with n-th order chemical reaction and Newtonian heating in porous medium”, *J. Porous Med.*, **22**(9), pp. 1141–1157 (2019).
  20. Animasaun, I., Koriko, O., Adegbe, K., et al. “Comparative analysis between 36 nm and 47 nm alumina-water nanofluid flows in the presence of Hall effect”, *Journal of Thermal Analysis and Calorimetry*, **135**(2), pp. 873–886 (2019).
  21. Shah, S., Rafiq, N., Abdullah, F.A., et al. “Slip and radiative effects on MHD Maxwell nanofluid with non-Fourier and non-Fick laws in a porous medium”, *Case Studies in Thermal Engineering*, **30**, p. 101779 (2022).
  22. Carreau, P.J. “Rheological equations from molecular network theories”, *Transactions of the Society of Rheology*, **16**(1), pp. 99–127 (1972).
  23. Bird, R.B., Stewart, W.E., and Lightfoot, E.N., *Transport Phenomena*, John Wiley and Sons, Inc., New York (1960).
  24. Atif, S.M., Hussain, S., and Sagheer, M. “Numerical study of MHD micropolar Carreau nanofluid in the presence of induced magnetic field”, *AIP Advances*, **8**, 035219 (2018).
  25. Hashim and Khan, M. “A revised model to analyze the heat and mass transfer mechanisms in the flow of Carreau nanofluids”, *International Journal of Heat and Mass Transfer*, **103**, pp. 291–297 (2016).
  26. Khan, M., Malik, M., Salahuddin, T., et al. “Numerical modeling of Carreau fluid due to variable thicked surface”, *Results in Physics*, **7**, pp. 2384–2390 (2017).
  27. Martins, R., Silveira, F., and Martins, M. “Numerical investigation of inertia and shear thinning effects in axisymmetric flows of Carreau fluids by a Galerkin least-squares method”, *Latin American Applied Research*, **38**(4), pp. 321–328 (2008).
  28. Olajuwon, I.B. “Convection heat and mass transfer in a hydromagnetic Carreau fluid past a vertical porous plate in presence of thermal radiation and thermal diffusion”, *Thermal Science*, **15**(2), pp. 241–252 (2011).
  29. Atif, S.M., Hussain, S., and Sagheer, M. “Effect of thermal radiation and variable thermal conductivity on magnetohydrodynamics squeezed flow of Carreau fluid over a sensor surface”, *Journal of Nanofluid*, **8**, pp. 806–816 (2019).
  30. Tshela, M.S. “The flow of Carreau fluid down an incline with a free surface”, *International Journal of Physical Sciences*, **6**, pp. 3896–3910 (2011).
  31. Alsemiry, R.D., Sayed, H.M., and Amin, N. “Mathematical analysis of Carreau fluid flow and heat transfer within an eccentric catheterized artery”, *Alexandria Engineering Journal*, **61**, pp. 523–539 (2022).
  32. Reedy, C.S., Srihari, P., Ali, F., et al. “Numerical analysis of Carreau fluid flow over a vertical porous microchannel with entropy generation”, *Partial Differential Equations in Applied Mathematics*, **5**, p. 100304 (2022).
  33. Thangavelu, M., Nagarajan, N., Oztop, H.F., et al. “MHD convection flow of Ag-water nanofluid in inclined enclosure with center heater”, *Journal of Mechanics*, **37**, pp. 13–27 (2020).
  34. Selimli, S., Recebli, Z., and Arcaklioglu, E. “MHD numerical analyses of hydrodynamically developing laminar liquid lithium duct flow”, *International Journal of Hydrogen Energy*, **40**(44), pp. 15358–15364 (2015).
  35. Idowu, A.S., Akolade, M.T., Abubakar, J.U., et al. “MHD free convective heat and mass transfer flow of dissipative Casson fluid with variable viscosity and thermal conductivity effects”, *Journal of Taibah University for Science*, **14**(1), pp. 851–862 (2020).
  36. Selimli, S., Recebli, Z., and Arcaklioglu, E. “Combined effects of magnetic and electrical field on the hydrodynamic and thermophysical parameters of magnetoviscous fluid flow”, *International Journal of Heat and Mass Transfer*, **86**, pp. 426–432 (2015).

37. Iqbal, M.S., Mustafa, I., Riaz, I., et al. “Influence of carbon nanotubes on heat transfer in MHD nanofluid flow over a stretchable rotating disk: A numerical study”, *Heat Transfer*, **50**(1), pp. 619–637 (2021).
38. Gupta, S., Gupta, S., and Sharma, A. “Darcy Forchheimer flow of MHD Jeffrey nanofluid over a permeable cone with Cattaneo-Christov heat and mass flux theories”, *Indian Journal of Physics*, **96**, pp. 503–513 (2022).
39. Gopal, D., Saleem, S., Jagadha, S., et al. “Numerical analysis of higher order chemical reaction on electrically MHD nanofluid under influence of viscous dissipation”, *Alexandria Engineering Journal*, **60**(1), pp. 1861–1871 (2021).
40. Waqas, H., Kafait, A., Alghamdi, M., et al. “Thermobioconvective transport of magneto-Casson nanofluid over a wedge containing motile microorganisms and variable thermal conductivity”, *Alexandria Engineering Journal*, **61**(3), pp. 2444–2454 (2022).
41. Rout, B. and Mishra, S. “Thermal energy transport on MHD nanofluid flow over a stretching surface: A comparative study”, *Engineering Science and Technology, an International Journal*, **21**(1), pp. 60–69 (2018).
42. Eid, M.R., Mahny, K., Dar, A., et al. “Numerical study for Carreau nanofluid flow over a convectively heated nonlinear stretching surface with chemically reactive species”, *Physica A: Statistical Mechanics and its Applications*, **540**, p. 123063 (2020).

## Biographies

**Shafqat Hussain** completed his PhD degree from Technische Universitat (TU) Dortmund, Dortmund,

Germany in 2012. He also worked as a visiting Assistant Professor at Ruhr-Universitat Bochum (RUB), Bochum, Germany. Currently, he is working as a Professor at Capital University of Science and Technology, Islamabad, Pakistan. Dr. Hussain has more than 100 publications in reputable journals. His research areas are mainly computational fluid dynamics using finite element methods, Krylov subspace, and multigrid iterative methods.

**Shahzada Muhammad Atif** completed his PhD from Capital University of Science and Technology, Islamabad, Pakistan in 2020 in Computational Fluid Dynamics. Dr. Atif has more than 15 publications in reputable journals. His research interests are fluid dynamics, magnetohydrodynamics, and properties of nanofluids and their heat transfer characteristics.

**Muhammad Sagheer** completed his PhD degree from Sussex University, England in 2005. Currently, he is the Head of Mathematics Department at Capital University of Science and Technology, Islamabad, Pakistan. Dr. Sagheer has more than 50 publications in reputable journals. His areas of interest include fluid dynamics, computational mathematics, eigenvalue problems, and computational biology.

**Muhammad Adnan Manzoor** is a research scholar at Capital University of Science and Technology, Pakistan. Currently, he is working at the Education Department of Azad Jammu & Kashmir. His research interests are fluid dynamics as well as properties of nanofluids and their heat transfer characteristics.